

Oxazolidine Derivatives as Corrosion Inhibitors for API X60 Steel in 1 M HCl Solution: Experimental and Theoretical Studies

Nuha Wazzan^{1,*}, I. B. Obot², Hassan Faidallah¹

¹ King Abdulaziz University, College of Science, Chemistry Department, Jeddah, Saudi Arabia

² Centre of Research Excellence in Corrosion, Research Institute, King Fahd University of Petroleum and Minerals, Dhahran 31261, Saudi Arabia

*E-Mail: nwazzan@kau.edu.sa

Received: 13 January 2019 / Accepted: 3 April 2019 / Published: 30 June 2019

Some synthesized oxazolidine derivatives (1-oxa-4-azaspiro [4,4]nonane, 1-oxa-4-azaspiro [4,5]decane, 6-methyl-1-oxa-4-azaspiro [4,5]decane and 1-oxa-4-azaspiro [4,7]dodecane) have been tested as promising inhibitors for API 5L X60 steel corrosion in a 1 M HCl solution using weight loss and electrochemical techniques complemented with computational studies. Characterization of the synthesized compounds was achieved using ¹H and ¹³C NMR spectroscopic analysis. The oxazolidine derivatives could efficiently lower the corrosion rate of the steel sample during 24 h of immersion in an acidic medium. The oxazolidine derivatives have minimal effect on the corrosion potential of steel in the acid solution. Their adsorption onto the steel surface effectively improved the charge transfer resistance, and the oxazolidine compounds acted as mixed-type inhibitors. A cyclooctyl substitution at the C-11 position produced the highest inhibitor efficiency, and attachment of a methyl group could enhance the inhibition efficiency of the cyclohexyl substituent at the C-11 position. Density functional theory calculations were conducted to gain insight into the structural and electronic properties of the four corrosion inhibitors and their inhibitory effects.

Keywords: Oxazolidine Derivatives; Electrochemistry; Corrosion inhibitors; DFT; Steel; Acid corrosion.

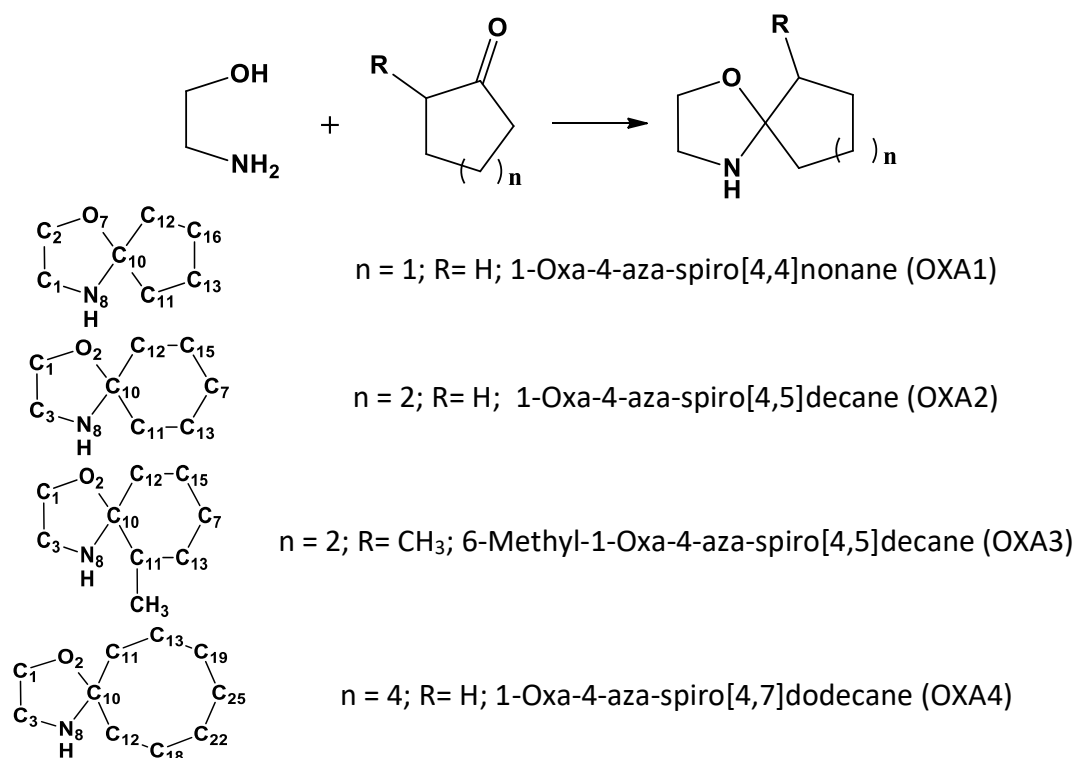
1. INTRODUCTION

Steel alloys continue to enjoy immense importance in many industries, such as desalination plants, refineries, manufacturing and even construction industries, due, practically, to properties such as high tensile strength, malleability, ductility and ready availability. Unfortunately, however, their application in these industries inevitably exposes them to regular contact with strong acids, such as hydrochloric acid (HCl), during practices such as descaling and pickling, which are practiced in these

industries. A major consequence of the steel–acid contact is severe corrosion attack, which leads to serious material damage and, subsequently, substantial financial loss. Although well-known techniques such as the application of surface coatings and selection of alloy materials have traditionally been utilized in many industries to prevent metallic corrosion, these techniques do not outperform the application of corrosion inhibitors, especially from organic sources, which offer greater advantages, such as environmental friendliness, cost effectiveness and excellent practicability in mitigating steel acid corrosion. The literature contains extensive works that have been reported in this regard [1-13]. In addition to being derived from plant extracts, many effective organic corrosion inhibitors that have been studied are also drug-related substances [14-16]. These organic corrosion inhibitors contain moieties with π -electrons and non-bonding electrons, such as double or triple bonds or heteroatoms such as nitrogen, oxygen or sulfur. Inhibition chemistry involves using the heteroatoms as anchor points for adsorption onto active sites of the alloy, leading to the formation of inert barrier layers between the surface and the acid solution [17, 18]. In addition, a recent review by [19] emphasized that the spatial orientation of the inhibitor molecules also exerts some influence on the efficiency of inhibition by a given molecule.

Oxazolidine (1,3-oxazolidine) is the reduced form of oxazoline and possesses nitrogen and oxygen heteroatoms separated by a carbon atom in a heterocyclic structure. Oxazolidine-based compounds have attracted attention as a new class of orally active synthetic antibiotics with a unique mechanism of bacterial protein synthesis inhibition [20-22]. A special class of oxazolidine derivatives includes oxa–azaspiro compounds, which have been reported for their immense application in the treatment of cancer [23, 24], convulsion [25, 26], dermatitis [27], tuberculosis [28] and Alzheimer's disease [29]. The excellent medicinal properties of these oxazolidine derivatives are strongly related to their heterocyclic nitrogen functionality. In addition to the oxygen functionality contained in the oxa–azaspiro compounds, it is thought that these oxazolidine derivatives can exhibit good corrosion inhibition properties. Unfortunately, such reports are seriously lacking in the literature. The only available work is that reported in [30], where some isoxazolidine derivatives were shown to be effective inhibitors against the corrosion API 5L X60 steel in a 1 M HCl solution.

In the present research, we investigate the ability of some oxazolidine derivatives, namely, 1–oxa–4–azaspiro compounds, to serve as API 5L X60 steel corrosion inhibitors in a 1 M HCl solution using weight loss and electrochemical techniques in conjunction with computational calculations to elucidate the electronic properties of the inhibitors related to the adsorption and binding characteristics of the molecules on the steel surface. The compounds include 1–oxa–4–azaspiro [4,4]nonane, 1–oxa–4–azaspiro [4,5]decane, 6–methyl–1–oxa–4–azaspiro [4,5]decane and 1–oxa–4–azaspiro [4,7]dodecane and have been coded as OXA1, OXA2, OXA3 and OXA4, respectively, in the present report (see Scheme 1). It is envisaged that the results from this work will contribute to the increasing literature in the continuous design of effective corrosion inhibitors, especially for steel alloys in acidic media.



Scheme 1. Synthetic route for the oxazolidine-based inhibitors along with their IUPAC names and atomic numbering used throughout this study

2. EXPERIMENTAL

2.1. Synthesis and characterization of the oxazolidine derivatives

The laboratory synthesis was carried out by following a previously reported procedure [31]. The chemicals employed in the synthesis of the oxazolidine derivatives were analytical grade reagents obtained from Sigma Aldrich and were used as purchased without further purification. Scheme 1 shows the synthetic route for the oxazolidine derivatives (OXA1 to OXA4). The synthesis process involved refluxing a mixture of ethanolamine and the appropriate ketone in dry benzene for an appropriate amount of time (until no water more was collected). Then, column chromatography on a silica gel was used to remove the benzene. Characterization of the four synthesized oxazolidine derivatives was performed using ¹H and ¹³C NMR spectroscopy using tetramethyl silane as an internal standard and deuterated DMSO as the solvent. Moreover, the characterization process also involved the use of elemental analyses, followed by checking the homogeneity of the compounds by TLC, where the spots were detected by exposure to ultraviolet lamp at $\lambda = 254 \text{ nm}$. The details of the procedures used in the synthesis and characterization processes have been reported in our previous publication [32].

2.2. Weight loss measurements

Weight loss measurements were performed according to the ASTM standard. API 5L X60 steel coupons with dimensions of 3 cm × 3 cm × 1 cm were abraded to a final grit size of 800 using silicon

carbide paper, washed with distilled water, ultrasonically degreased in acetone for 10 min and thereafter dried with warm air using a mechanical drier. The test acid solution (1 M HCl) was prepared by diluting an appropriate volume of 37 % concentrated HCl (Sigma Aldrich) with double distilled water. The steel coupons were weighed and immersed in the acid solution for 24 h at 25 °C without and with 0.5 % inhibitors. After 24 h, the coupons were retrieved, quickly immersed in the 1 M HCl solution for 10 s to remove the corrosion products, thoroughly washed with distilled water and ultrasonically cleaned in acetone for 10 min, followed by warm air drying. The coupons were then reweighed to extrapolate the weight loss that occurred during immersion. Given an exposed surface area ($A \text{ cm}^2$), the density of the steel sample (ρ) and the time of immersion (t), the corrosion rate in mm per year (mpy) was calculated from the weight loss (ΔW) of the steel samples according to Equation (1). Subsequently, the inhibition efficiency (IE %) from weight loss measurements was calculated according to Equation (2), where $C_{R(\text{blank})}$ and $C_{R(\text{inh})}$ are, respectively, the corrosion rates in the absence and presence of an inhibitor.

$$\text{Corrosion rate (mpy)} = \frac{\Delta W \times 87.6}{\rho \times A \times t} \quad (1)$$

$$\text{IE \%} = \frac{[C_{R(\text{blank})} - C_{R(\text{inh})}]}{C_{R(\text{blank})}} \times 100 \quad (2)$$

2.2. Electrochemical measurements

All electrochemical measurements were performed under naturally aerated conditions after the working electrode was freely immersed for 1 h in the appropriate test solutions, during which an open circuit potential (OCP) must have been attained based on previous reports [30, 33]. Subsequently, EIS measurements were carried out in the frequency range of 100 kHz to 0.01 Hz using a voltage amplitude of 10 mV. The potentiodynamic polarization (PDP) measurements were recorded within a potential perturbation range of ± 250 mV with respect to the free corrosion potential (E_{corr}) by applying a scan rate of 0.5 mV/s. Polarization parameters such as E_{corr} , i_{corr} and Tafel constants were derived based on the Tafel extrapolation method. Linear polarization resistance (LPR) measurements were performed within ± 10 mV of the E_{corr} using a scan rate of 0.167 mV/s. Calculation of the inhibition efficiency (IE %) from the electrochemical measurements was performed using Equations (3) to (5). A similar procedure for conducting the electrochemical experiment has been reported in our previous publications [32, 34].

$$IE_{EIS} = 1 - \frac{R_{ct(\text{blank})}}{R_{ct(\text{inh})}} \times 100 \quad (3)$$

where $R_{ct(\text{blank})}$ and $R_{ct(\text{inh})}$ are, respectively, the charge transfer resistances recorded in the absence and presence of an inhibitor;

$$IE_{PDP} = 1 - \frac{i_{\text{corr}(\text{inh})}}{i_{\text{corr}(\text{blank})}} \times 100 \quad (4)$$

where $i_{\text{corr}(\text{blank})}$ and $i_{\text{corr}(\text{inh})}$ are, respectively, the corrosion current densities recorded in the absence and presence of an inhibitor; and

$$IE_{LPR} = 1 - \frac{R_{p(\text{blank})}}{R_{p(\text{inh})}} \times 100 \quad (5)$$

where R_p (blank) and R_p (inh) are, respectively, the polarization resistances recorded in the absence and presence of an inhibitor.

2.4. Computational studies

The Gaussian 09 package [35] was used to perform density functional theory (DFT) calculations, with Becke's three parameter exchange functional along with the Lee–Yang–Parr nonlocal correlation functional (B3LYP) [36, 37] and the 6-311++G(d,p) basis set. Since electrochemical corrosion generally occurs in aqueous solutions, the polarizable conductor calculation model (CPCM) was used to simulate water as a solvent [38, 39].

3. RESULTS AND DISCUSSION

3.1. Synthesis and characterization of the oxazolidine derivatives

Scheme 1 shows the synthesis route for oxazolidine derivatives OXA1 to OXA4, which were obtained via cyclocondensation of ethanolamine with the appropriate ketones using a Dean-Stark trap. The synthesis method afforded the corresponding oxazolidine derivatives in good yields (78 – 86 %). The ^1H NMR spectra of OXA1 to OXA4 showed two sets of triplets at δ 2.55–3.43 and δ 3.00–3.76 that were attributed to the intensity of two protons at the H-3 and H-2 positions, respectively. An exchangeable broad singlet at δ 7.3–7.68 attributed to NH was also observed. The cyclic aliphatic hydrogen atoms produced different kinds of signals for the various oxazolidine derivatives. These signals include two triplets at δ 1.61 and 1.73 corresponding to 8H in OXA1 and several multiplet peaks between δ 1.33 and 1.59 attributed to 10H for OXA2, between δ 1.38 and 1.57 attributed to 9H for OXA3 and between δ 1.32 and 1.76 attributed to 14H in OXA4. In addition, a single peak at δ 1.09 was observed only for OXA3, representing the three equal hydrogen atoms of the CH_3 group attached to the cyclohexyl substituent. In addition, the ^{13}C NMR spectra exhibited singlet peaks at δ 61.98, 64.12, 65.02 and 68.69 due to the C-2 carbon in the oxazolidine base molecule. While OXA1 yielded only two peaks at δ 23.64 and δ 35.54 due to the cyclic aliphatic carbon, the other oxazolidine derivatives produced three sets of singlet peaks at δ 23.74, 25.65, and 35.63 for OXA2; at δ 23.66, 25.88, and 35.07 for OXA3; and at δ 22.52, 29.92, and 41.34 for OXA4. Again, only OXA3 showed a peak at δ 14.94 due to the methyl group attached to the cyclohexyl substituent.

3.2. Weight loss measurement

The corrosion rate of the API 5L X60 steel sample in a 1 M HCl solution without and with oxazolidine derivatives OXA1 to OXA4 is strongly correlated with the change in mass of the weighed steel sample before and after the 24 h of immersion. According to Table 1, the steel sample in the 1 M HCl solution without an inhibitor experienced a greater weight loss than the samples in the presence of any of the inhibitors. The presence of the oxazolidine inhibitors, therefore, definitely decreased the

corrosion rate of the X60 steel in the 1 M HCl solution. This phenomenon is readily attributed to coverage of the steel surface by the oxazolidine-based compounds via adsorption, which ultimately protects the surface from attack by the acid solution [40, 41]. The efficiency of inhibition for the compounds followed the order OXA2 < OXA3 < OXA1 < OXA4 with respective IE % values of 43.64 %, 52.73 %, 66.06 % and 72.12 %. This indicates that 1-oxa-4-azaspiro [4,7]dodecane can provide the greatest surface coverage of the steel sample, while 1-oxa-4-azaspiro [4,5]decane provides the least surface coverage compared with the other oxazolidine derivatives studied. Given that the inhibition efficiency of organic corrosion inhibitors is strongly correlated with the extent of their adsorption on the surface of the corroding metallic material, the adsorption must also be influenced by the internal energy of the inhibitor molecules, which controls their reactivity. Such energy should also be controlled by the strain energy of the substituents attached to the oxazolidine parent molecule. According to the other reports [42], the cyclooctyl substituent possesses a higher strain energy than the other substituents attached to the oxazolidine moiety, while the strain energy of the cyclopentane is greater than that of cyclohexane. This is consistent with the observed inhibitor efficiency displayed by the oxazolidine derivatives. Relative to OXA2, which has a cyclohexyl substituent, OXA3 (which has a methyl group attached to the cyclohexyl substituent) displays a greater efficiency, which is definitely attributed to the electron-donating power of the methyl group [43].

Table 1. Corrosion parameters derived from the weight loss experiment for API 5L X60 steel immersed for 24 h in a 1 M HCl solution without and with 0.5 % synthesized oxazolidine derivatives

System	Average Weight loss (g)	Corrosion Rate (mpy)	Inhibition Efficiency (%)
Blank	0.00825	20.12	–
OXA1	0.00280	6.83	66
OXA2	0.00465	11.34	44
OXA3	0.00390	9.51	53
OXA4	0.00230	5.61	72

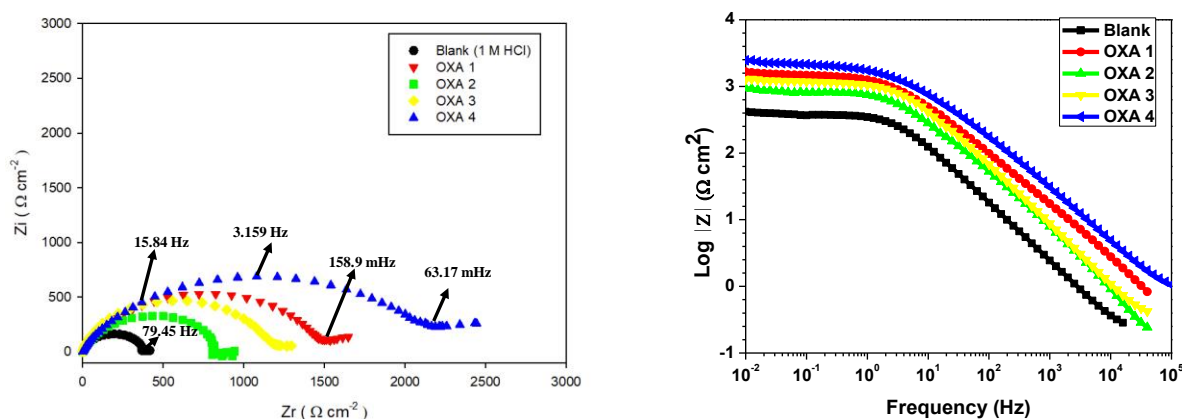
3.3. Electrochemical Impedance Spectroscopy (EIS)

EIS analysis can elucidate how the oxazolidine derivatives influence the kinetics and mechanism of the API 5L X60 steel corrosion in a 1 M HCl solution. After 1 h of stable OCP attainment, the EIS results for the steel sample in the acid solution without and with the corrosion inhibitors are displayed in the form of Nyquist and Bode modulus plots, as represented in Figure 1. The Nyquist plots (Figure 1 (a)) reveal incomplete semicircles for the steel in the absence and presence of the corrosion inhibitors, which indicates that the oxazolidine derivatives did not change the corrosion mechanism of the steel in the 1 M HCl solution but resulted in evident modification based on the changes in the sizes of the semicircular arcs. The increased size of the semicircles in the presence of the inhibitors corroborates the finding from the weight loss experiments, indicating that the oxazolidone inhibitors increase the corrosion resistance of API 5L X60 steel in a 1 M HCl solution. Similarly, the values of absolute impedance, based on the BODE modulus plots in Figure 1 (b), exhibited by the steel sample greatly

increased during the frequency scan in the presence of the inhibitors compared with the blank HCl solution. The single impedance loops displayed in the Nyquist plots throughout the steel corrosion in the absence and presence of the inhibitors indicate that the electrochemical corrosion mechanism of the steel sample in 1 M HCl solutions without and with the oxazolidine inhibitors was controlled by the capacitance at the steel surface–acid solution interface and the resistance to charge transfer across the interface. Hence, the one-time constant represented by the equivalent circuit in Figure 1 (c) was adopted to model the impedance behavior of the API 5L X60 steel corrosion in 1 M HCl solutions without and with the oxazolidine inhibitors. A similar equivalent circuit model was adopted in previous works for the corrosion of steel alloys in HCl solutions without and with some organic corrosion inhibitors [1, 44, 45]. In the model, R_s is the solution resistance, CPE_{dl} is the double-layer capacitance of a constant phase element, and R_{ct} is the resistance to charge transfer across the interface. The constant phase element, CPE, has been used instead of a pure capacitor to compensate for the surface inhomogeneity of solid electrode materials, which usually exhibit frequency-dependent dispersions [32]. The impedance of a constant phase element, Z_{CPE} , is given by Equation 6, where Y_0 is the admittance, n is the CPE exponent, $j = (-1)^{\frac{1}{2}}$ is an imaginary number ω is the angular frequency in rad./s.

$$Z_{CPE} = Y_0^{-1} (j\omega)^{-n} \tag{6}$$

The corresponding electrical parameters derived from the model are presented in Table 2. The R_{ct} values, which are a measure of the corrosion resistance of a steel sample in an HCl solution, generally increased in the presence of the oxazolidine derivatives. The R_{ct} and IE % values calculated from R_{ct} also followed a similar trend of OXA2 < OXA3 < OXA1 < OXA4. The Y_0 values decreased in the presence of the inhibitors compared with the value for the blank solution. Equation 6 shows that the Y_0 value varies inversely with the impedance of the sample. Thus, the impedance of the steel sample increased in the presence of the oxazolidine derivatives and was highest in the presence of the OXA4 compound, corroborating the experimental findings and following a similar trend as observed from the weight loss experiment. The accuracy of the equivalent circuit chosen to model the impedance behavior of the steel corrosion was verified based on the excellent overlap of the experimental and fitting plots, according to Figure 1 (d) and based on the values of the goodness of fit in Table 2.



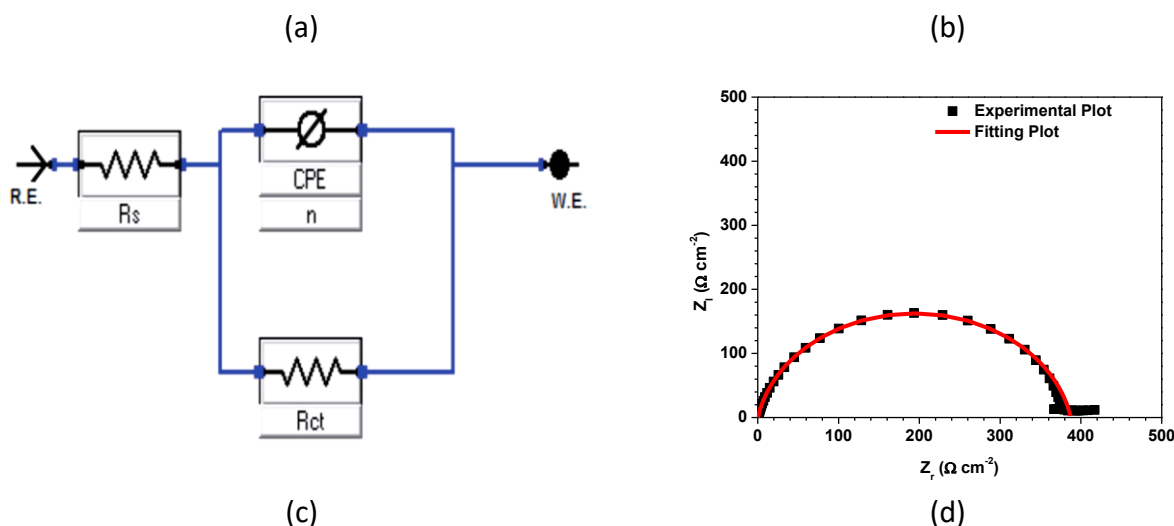


Figure 1. EIS plots for API 5L X60 steel in 1 M HCl solutions without and with 0.5 % synthesized oxazolidine derivatives expressed in (a) Nyquist and (b) absolute impedance formats, along with (c) an equivalent circuit model and (d) fitting plots.

Table 2. EIS parameters of API 5L X60 steel after corrosion in 1 M HCl solutions without and with 0.5 % synthesized oxazolidine derivatives

System	R_s ($\Omega \text{ cm}^{-2}$)	Y_o ($\mu\Omega \text{ S}^n \text{ cm}^{-2}$)	$R_{ct} (\times 10^3)$ ($\Omega \text{ cm}^2$)	N	Goodness of Fit ($\times 10^{-3}$)	IE %
Blank	0.19	180	0.38	0.9	9.42	–
OXA1	0.42	66	1.53	0.8	2.09	75
OXA2	0.69	75	0.83	0.9	1.60	53
OXA3	0.48	69	1.17	0.9	4.18	67
OXA4	0.55	40	2.14	0.8	8.52	82

3.4. Linear Polarization Resistance (LPR)

Instantaneous corrosion rate information concerning the effect of the oxazolidine derivatives on steel corrosion in a 1 M HCl solution was acquired from linear polarization resistance (LPR) measurements. A safe potential perturbation was applied to displace the sample within ± 10 mV of its open circuit potential (OCP) position. Within this potential range, it has been reported that the relatively steady state assumed by the corroding sample is not disturbed, that a linear relationship exists between the applied overpotential and the resultant current density response, and that the polarization resistance, R_p , can be extrapolated from the slope of the potential–current plot [46, 47]. The X60 steel sample was allowed to attain an OCP during 1 h of free corrosion in the 1 M HCl solutions without and with 0.5 % of the oxazolidine derivatives, and the results of the subsequent LPR measurements are presented in Table 3. The polarization resistance, R_p , was calculated from the slope of the potential vs current plot by assuming anodic and cathodic Tafel constants of 0.12 V/decade. The addition of the oxazolidine inhibitors showed no significant change in the corrosion potential (E_{corr}) of the steel sample in the acid solution. However, their presence obviously increased the R_p value for the steel corrosion, as the R_p value shifted from $481 \Omega \text{ cm}^{-2}$ in the blank HCl solution and increased according to the order OXA2 <

OXA3 < OXA1 < OXA4, reaching a maximum R_p value in the presence of the OXA4 inhibitor. Similarly, the IE % value calculated for the inhibitors reached a maximum of greater than 81 % in the presence of OXA4. Thus, regardless of the order of corrosion inhibition, the present result reveals that the oxazolidine derivatives are excellent inhibitors for X60 steel corrosion in 1 M HCl solutions. This is very consistent with the EIS results.

Table 3. Linear polarization results for API 5L X60 steel in 1 M HCl solutions without and with 0.5 % oxazolidine derivatives

System	E_{corr} (mV/Ag/AgCl)	R_p ($\Omega \text{ cm}^{-2}$)	IE %
Blank	-452	481	–
OXA1	-466	1676	71
OXA2	-454	1187	59
OXA3	-462	1378	65
OXA4	-457	2612	82

3.5. Polarization techniques

Potentiodynamic polarization (PDP) was deployed to further understand how the oxazolidine derivatives influenced the kinetics of anodic and cathodic half-reactions occurring on the steel surface during corrosion in the 1 M HCl solution. The PDP plots derived for the X60 steel sample in the acid solution without and with 0.5 % oxazolidine derivatives are provided in Figure 2. The addition of the OXA1 to OXA4 inhibitors to the HCl solution did not change the corrosion mechanism of the steel in the acid solution, given the weak deviation of the E_{corr} values and the salient similarities in the shapes of the polarization curves, which can generally be interpreted to involve active dissolution without a transition to passivation. The oxazolidine derivatives inhibited both the anodic and cathodic half-reactions during steel corrosion, which implies that they function as mixed inhibitors. The obvious differences between the β_a and β_c values in the inhibited solution and the blank also affirm that the inhibitors are mixed-type inhibitors. A similar mechanism was reported when some isoxazolidine derivatives were investigated as corrosion inhibitors for a similar kind of X60 steel in a 1 M HCl solution [30]. Indeed, the reduction in the cathodic and anodic currents was most prominent in the presence of the OXA4 inhibitor, followed by OXA1, so the inhibition trend for the oxazolidine derivatives remained consistent with the observations from weight loss, EIS and LPR experiments. This is further elucidated from the electrical parameters (E_{corr} , i_{corr} , β_a and β_c) derived from the PDP plots using the Tafel extrapolation, as detailed in Table 4. The i_{corr} values are measures of the corrosion rate of the steel sample. The lower i_{corr} values obtained in the presence of the inhibitors relative to the blank solution indicate that the oxazolidine derivatives are effective inhibitors against the corrosion of X60 steel in a 1 M HCl solution.

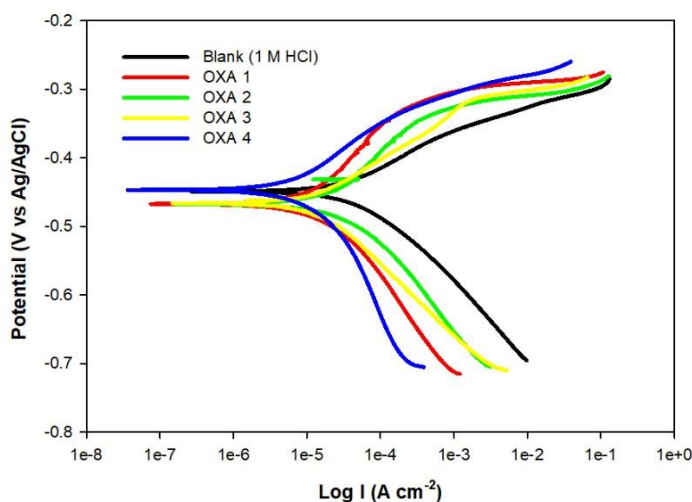


Figure 2. Potentiodynamic polarization plots for API 5L X60 steel in 1 M HCl solutions without and with 0.5 % synthesized oxazolidine derivatives

Table 4. Polarization parameters for API 5L X60 steel after corrosion in 1 M HCl solutions without and with 0.5 % synthesized oxazolidine derivatives

System	E_{corr} (mV/Ag/AgCl)	i_{corr} $\mu\text{A cm}^{-2}$	β_a mV dec^{-1}	β_c mV dec^{-1}	IE%
Blank	-449	37.80	69.3	82.8	-
OXA1	-467	15.10	196.5	138.3	60
OXA2	-468	31.50	139.5	101.5	17
OXA3	-433	20.70	104.1	202.9	45
OXA4	-450	10.70	124.9	147.6	72

3.6 Computational studies

3.6.1 Global descriptors

The structures of the investigated inhibitors were optimized in the gas phase and aqueous solution using B3LYP/ and CPCM/B3LYP/6-311++G(d,p), respectively. The optimized electronic structures are minima on the potential energy surface (PES) with no imaginary frequencies. Based on frontier molecular orbital (FMO) theory and Fukui's theory, the ability of a molecule to donate electron/s is controlled by the HOMO level. Since a higher E_{HOMO} value allows the molecule to donate electrons easily to an acceptor molecule/atom (such as the unfilled d-orbital of the Fe atom in the corrosion case), this will enhance the adsorption process between the inhibitor and the metal surface [48]. In contrast, the ability of the inhibitor molecule to receive electrons during the electron back-donation process from the filled d-orbital of the Fe atom to the inhibitor is facilitated by a lower LUMO level of the inhibitor molecule. Therefore, a lower E_{LUMO} will enhance the adsorption process. Consequently, the gap between the HOMO and LUMO energy levels of the molecules ($\Delta E = E_{\text{LUMO}} - E_{\text{HOMO}}$) is an important descriptor. This gap corresponds to the ability to donate and accept electrons during the adsorption

process. Figure 3 shows the optimized geometries, the spatial distribution of the FMOs (HOMO and LUMO), and the molecular electrostatic potential (ESP) of the investigated inhibitors.

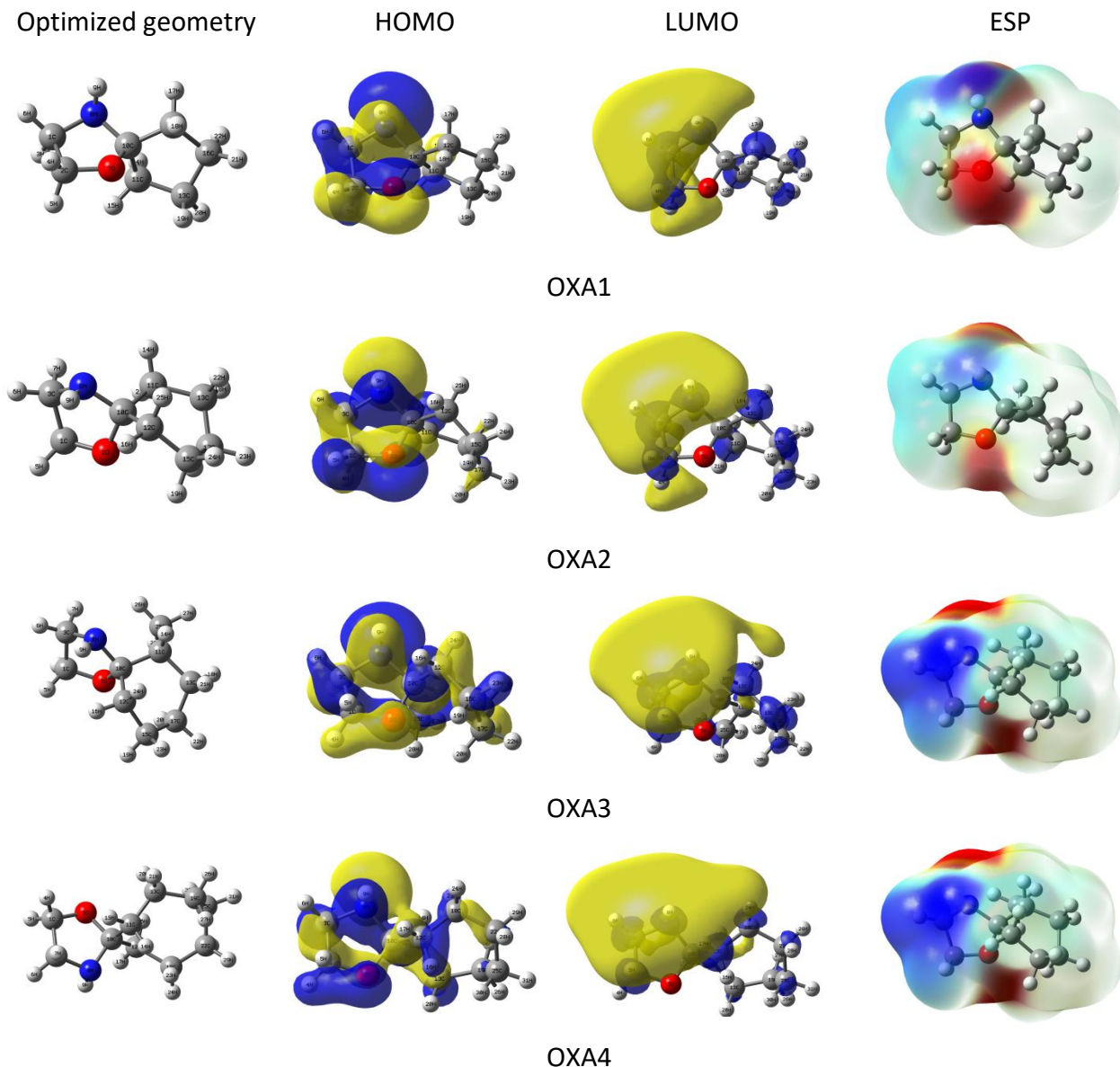


Figure 3. Optimized geometries, spatial distributions of the HOMOs and LUMOs, and electrostatic potential of investigated inhibitors in the gas phase

Figure 3 shows that the HOMOs of the four molecules are delocalized over the oxazolidine ring and on C11 in OXA1 and OXA2. However, the HOMO is delocalized over the entire skeleton of OXA3, *i.e.*, the oxazolidine and methylcyclohexane rings. Therefore, the presence of the methyl group at C11 of the cyclohexane ring significantly affects the HOMO distribution. The delocalization of the HOMO of OXA4 is somewhat intermediate between its distribution on the whole OXA3 skeleton and its distribution mainly on the oxazolidine ring of the OXA1 and OXA2 molecules. In contrast, the LUMOs show significant delocalization on the oxazolidine ring, except on the O2/7 atom of this ring. Additionally, the LUMO is distributed partially on the other ring (cyclopentane, cyclohexane, methylcyclohexane, and cyclooctane in the OXA1, OXA2, OXA3, and OXA4, respectively).

Table 5. The quantum chemical parameters of the investigated inhibitors in the gas phase

Inhibitor	E_{HOMO}	E_{LUMO}	IP	EA	ΔE	χ	η	σ	ω	ε	RE
OXA1	-6.784	-0.285	6.784	0.285	6.499	3.534	3.249	0.308	7.382	0.135	117.96
OXA2	-6.737	-0.306	6.737	0.306	6.431	3.521	3.215	0.311	7.084	0.141	78.64
OXA3	-6.501	-0.356	6.501	0.356	6.145	3.429	3.073	0.325	14.172	0.071	39.32
OXA4	-6.733	-0.318	6.733	0.318	6.415	3.526	3.207	0.312	6.798	0.147	0.00

Table 6. The quantum chemical parameters of the investigated inhibitors in aqueous solution

Inhibitor	E_{HOMO}	E_{LUMO}	IP	EA	ΔE	χ	η	σ	ω	ε	RE
OXA1	-6.932	-0.207	6.932	0.207	6.725	3.570	3.362	0.297	9.724	0.103	117.96
OXA2	-6.874	-0.238	6.874	0.238	6.637	3.556	3.318	0.301	8.850	0.113	78.64
OXA3	-6.614	-0.245	6.614	0.245	6.369	3.430	3.185	0.314	18.495	0.054	39.32
OXA4	-6.892	-0.226	6.892	0.226	6.666	3.559	3.333	0.300	8.871	0.113	0.00

As reported [49-51], there are strong relationships between some theoretical quantum chemical parameters (QCPs) and the experimental inhibition efficiencies. Such parameters are dependent on the HOMO and LUMO energies and are called global descriptors, including the global hardness (η), global softness (σ), and electronegativity (χ). Other parameters that are dependent on the aforementioned parameters and are very useful descriptors to justify/interpret the experimental inhibition efficiencies include the electrophilicity (ω) and nucleophilicity (ε), the fraction of electrons transferred (ΔN), the energy of back donation (ΔE_{b-d}), electronic charge accepting capability and the initial molecule-metal interaction energy ($\Delta\psi$). Table 5, Table 6, and Table 7 list the calculated QCPs for the four inhibitors in the gas phase and aqueous solution. The equations used to calculate these parameters can be found in the literature [48, 52, 53].

The presence of solvent does not substantially affect the electronic properties of the investigated inhibitors [54]. The QCPs display very similar trends in the gas phase and aqueous solution. However, the presence of water as a solvent stabilizes the HOMO levels and destabilizes the LUMO levels by no more than 0.2 eV [54]. This in turn leads to an increase in the hardness and electronegativity values in the aqueous solution compared to their values in the gas phase.

As seen from the weight loss and electrochemical experiments, the inhibition efficiencies (%IE) of the four molecules decrease in the following order: OXA4 \geq OXA1 > OXA3 \geq OXA2 (see Table 1, Table 2, Table 3, and Table 4). As shown in Table 5 and Table 6, it is notable that the E_{HOMO} value increases in the following order: OXA1 < OXA4 < OXA2 < OXA3. The OXA4 and OXA1 inhibitors, with the highest %IE values, have the lowest E_{HOMO} values, which does not correlate well since a higher HOMO energy should make it easier for the inhibitor to donate electron/s to the unfilled d -orbital of the Fe atom. Therefore, in this case, the HOMO energies of the molecules were not correlated very well with the experimental inhibition efficiencies. In terms of the LUMO energies, the E_{LUMO} values increase in the following order: OXA3 < OXA4 < OXA2 < OXA1. In contrast, a lower LUMO energy makes it easier for the inhibitor to accept electron/s from the filled d -orbital of the Fe atom; thus, OXA4, with the highest inhibition efficiency, has one of the lowest LUMO energies among the studied inhibitors. As reported, a molecule with a small energy gap may be more polarizable and thus more reactive and

kinetically less stable [48]. The data in Table 5 and Table 6 show that the ΔE values decrease in the following order: OXA1 > OXA2 > OXA4 > OXA3. Therefore, OXA4, with the maximum inhibition efficiency, shows one of the lowest energy gaps among the studied inhibitors. The weak correlations between the calculated E_{HOMO} and E_{LUMO} values and their gaps with the order of experimental inhibition efficiencies may be related to other factors, such as the difference in solubility of the investigated molecules. A similar conclusion was derived in the literature [55].

The electrophilicity index (ω) is a measure of the tendency of a molecule to gain electron/s. On the other hand, the nucleophilicity (ϵ), which is the inverse of ω , measures the ability to donate or share electron/s. As reported, smaller ω values and larger ϵ values are associated with good anticorrosive ability and *vice versa* [48]. As evident from Table 5 and Table 6, the order of increasing ω and decreasing ϵ values is OXA2 < OXA1 < OXA4 < OXA3. The inhibitors that have small electrophilicity index values are strong nucleophiles. However, there exists a discrepancy in the trend between the experimental inhibition efficiencies and the calculated ω and ϵ values: OXA3, as one of the least efficient inhibitors, has a larger ω value and is a weak nucleophile.

Table 7. Calculated fraction of electron transferred, initial molecule-Fe interaction energy, energy of back donation, and dipole moments of the investigated inhibitors

Inhibitor	Gas phase				Aqueous phase			
	ΔN	$\Delta\psi$	ΔE_{b-d}	μ	ΔN	$\Delta\psi$	ΔE_{b-d}	μ
OXA1	0.533	-0.924	-0.812	0.882	0.510	-0.875	-0.841	1.202
OXA2	0.541	-0.941	-0.804	0.837	0.519	-0.894	-0.830	1.079
OXA3	0.581	-1.038	-0.768	1.600	0.561	-1.001	-0.796	2.164
OXA4	0.542	-0.941	-0.802	0.801	0.516	-0.888	-0.833	1.087

It was showed that the experimental inhibition efficiencies of four 2-pyridyl-azole derivatives increase as the hardness increases and as the interaction energy between the inhibitor and surface of the metal increases due to the donation and back-donation process [56]. Therefore, if the electron donation and electron back-donation processes occur at the same time, the energy change is directly proportional to the hardness of the inhibitor molecule. As indicated in Table 5, Table 6, and Table 7, the hardness values are greater than zero and the energy of back donation (ΔE_{b-d}) values are smaller than zero in both the gas phase and aqueous solutions. Therefore, it is energetically favorable to donate electrons from the inhibitor to the metallic surface and back-donate these electrons in the reverse direction [57]. The η values of the investigated inhibitors increased in the order OXA3 < OXA4 < OXA2 < OXA1, while the ΔE_{b-d} values decreased in the reverse order, *i.e.*, OXA1 > OXA2 > OXA4 > OXA1.

As indicated in Table 7, the number of electrons transferred (ΔN) increases in the following order: OXA1 < OXA2 < OXA4 < OXA3. Thus, OXA4 and OXA1, the two inhibitors with the highest inhibition efficiencies, did not have the highest values of ΔN . This result did not agree well with the experimental results. However, according to Sanderson's electronegativity equalization principle [58], the equalization of the electronegativity of the inhibitor and metal surface will quench the process of charge transfer. The investigated inhibitors will most likely act as electron donors rather than electron acceptors, since their ΔN values are greater than zero. The initial molecule-Fe interaction energy ($\Delta\psi$)

values show a very similar trend to that observed for ΔN values [48, 54], as shown in Table 7. The dipole moments of the four inhibitors increase in the order OXA4 < OXA2 < OXA1 < OXA3. OXA4, with the highest inhibition efficiency corresponding to the minimum dipole moment; however, there is a discrepancy in the order of the calculated dipole moments and the experimental inhibition efficiencies. As proposed in the literature, the inverse correlation between the dipole moments and the inhibition efficiencies can be rationalized by the accumulation of inhibitor molecules with smaller dipole moment more favorably on the metal surface than inhibitor with large dipole moment value [59].

For the investigated inhibitors, most of their global molecular reactivity cannot be predicted accurately because these values are based solely on their HOMO and LUMO energies [48]; thus, it is necessary to take into account another extra condition to define their inhibitive ability; this will be discussed in the next sections by taking into account other reactivity descriptors (atomic charges and local reactivity descriptors).

3.6.2 Atomic charge

To calculate the charge distribution on each atom over the whole skeleton of the molecule, it is useful to use the Mulliken population and NBO analysis. The charge distribution on each atom could be used to predict the active site/s for the adsorption process. As reported, the heteroatom (O, S, and N) that is highly negatively charged is most likely the site that joins the inhibitor molecule to the metal surface (Fe, Cu, etc.) during the adsorption process in a donor-acceptor type reaction. Inhibitors show different inhibition efficiencies as a result of the presence of heteroatom/s in their molecular geometry [48, 55]. The calculated Mulliken and NBO charges of C, N and O atoms are presented in Table 8.

Table 8. Mulliken and NBO atomic charges and total negative charges (*TNC*) of C, N, and O atoms of the investigated inhibitors in the gas phase

OXA1			OXA2			OXA3			OXA4		
Atom	Mulliken	NBO	Atom	Mulliken	NBO	Atom	Mulliken	NBO	Atom	Mulliken	NBO
C1	-0.22	-0.22	C1	-0.02	-0.05	C1	0.03	-0.04	C1	0.01	-0.05
C2	-0.07	-0.05	O2	0.03	-0.64	O2	0.03	-0.64	O2	0.02	-0.63
O7	-0.01	-0.63	C3	-0.23	-0.22	C3	-0.25	-0.21	C3	-0.20	-0.21
N8	0.01	-0.67	N8	0.07	-0.67	N8	0.06	-0.69	N8	0.10	-0.68
C10	-0.69	0.46	C10	-0.97	0.46	C10	-0.99	0.49	C10	-1.52	0.47
C11	0.10	-0.42	C11	0.04	-0.41	C11	0.37	-0.24	C11	0.28	-0.41
C12	-0.58	-0.41	C12	-0.36	-0.40	C12	-0.22	-0.42	C12	-0.14	-0.41
C13	-0.36	-0.38	C13	-0.32	-0.38	C13	-0.23	-0.38	C13	-0.37	-0.39
C16	-0.29	-0.38	C15	-0.47	-0.38	C15	-0.42	-0.38	C18	-0.11	-0.39
			C17	-0.21	-0.39	C17	-0.40	-0.39	C19	-0.33	-0.38
						C25	-0.73	-0.57	C22	-0.55	-0.37
									C25	-0.24	-0.39
<i>TNG</i>	-2.22	-3.15		-2.58	-3.54		-3.24	-3.95		-6.70	-4.32

The calculations show that the nitrogen and oxygen atoms have positive Mulliken charge densities. The exception is O7 in the OXA1 molecule, which has a slightly negative charge (-0.01 au). In fact, high negative charge densities occur on the carbon atoms of the oxazolidine and other rings. All four molecules share the same number of heteroatoms (one O and one nitrogen), and these two atoms have partially positive charges. As indicated by the Mulliken charges, the active sites of the four molecules are the carbon atoms. It may be useful to calculate the total negative charge of each molecule (*TNG*); the *TNG* values increase as the number of carbon atoms increases, and the order of its increase is OXA1 (-2.22 au) < OXA2 (2.58 au) < OXA3 (-3.24 au) < OXA4 (-6.70 au). The molecule with the highest inhibition efficiency (OXA4) has the largest *TNG* value. On the other hand, the NBO charge analysis reveals that the heteroatoms (N and O) of the four molecules are negatively charged. The negative charges on the N and O atoms are slightly affected by the different geometries of the four inhibitors, ranging from -0.63 au to -0.69 au. Similarly, NBO shows that most of the carbon atoms in the two rings are also negatively charged. The exception is the C10 atom, where the two rings join together. Therefore, the NBO charges seem more capable of estimating the charges and explaining the experimental data and thus are used to calculate the Fukui indices (see below).

3.6.3 Local descriptors

To understand the local reactivity of the oxazolidine derivatives, the Fukui indices for each atom in the inhibitors were calculated at the B3LYP/6-31++G(d,p) level in the gas phase using the NBO charge distribution. The analysis of the Fukui indices and the local descriptors provides more information on the electrophilic and nucleophilic reactivity of a molecule [48]; the related data are collected in Table 9.

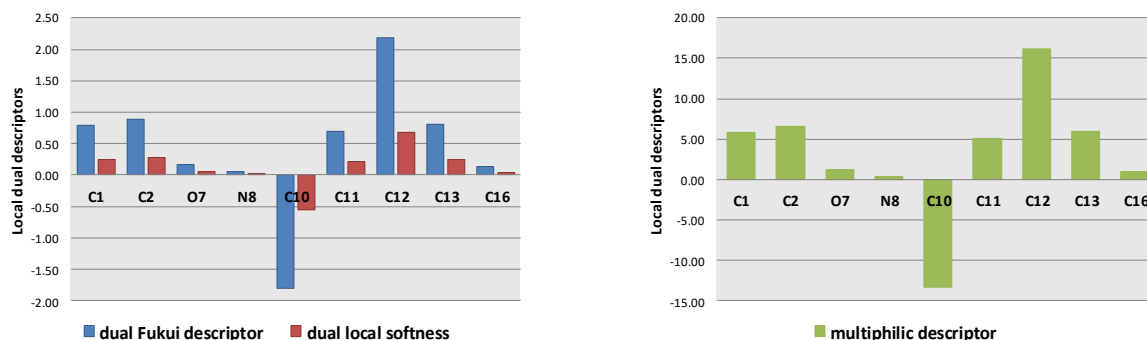
Table 9. Atomic Fukui indices of the investigated inhibitors in the gas phase

OXA1			OXA2			OXA3			OXA4		
Atom	f_k^+	f_k^-									
C1	-0.04	-0.83	C1	-0.02	0.68	C1	-0.04	0.34	C1	-0.03	-0.44
C2	-0.04	-0.93	O2	0.22	-0.03	O2	0.13	-0.05	O2	0.19	0.04
H3	0.09	0.21	C3	-0.05	0.70	C3	-0.01	0.66	C3	-0.04	-1.25
H4	0.12	0.41	H4	0.09	-0.30	H4	0.08	-0.25	H4	0.09	0.31
H5	0.10	0.44	H5	0.11	-0.24	H5	0.08	-0.13	H5	0.11	0.36
H6	0.09	1.28	H6	0.08	-0.99	H6	0.08	-1.11	H6	0.08	0.84
O7	0.23	0.05	H7	0.08	-0.01	H7	0.08	0.24	H7	0.09	0.37
N8	0.18	0.12	N8	0.18	-0.08	N8	0.19	-0.14	N8	0.22	0.05
H9	0.08	0.35	H9	0.07	-0.08	H9	0.08	-0.11	H9	0.08	0.22
C10	-0.20	1.61	C10	-0.21	-1.89	C10	-0.11	-1.82	C10	-0.30	0.98
C11	0.03	-0.66	C11	0.11	1.33	C11	-0.07	0.55	C11	0.04	-1.67
C12	0.07	-2.12	C12	-0.03	-0.36	C12	0.02	1.03	C12	0.06	-0.44
C13	0.02	-0.79	C13	-0.04	0.60	C13	-0.05	-0.15	C13	0.01	-0.26
H14	0.05	0.31	H14	0.05	-0.14	H14	0.05	0.02	H4	0.04	0.22

H15	0.03	0.21	C15	-0.02	0.87	C15	0.01	0.83	H15	0.02	-0.29
C16	-0.05	-0.18	H16	0.03	-0.18	H16	0.04	-0.47	H16	0.04	-0.10
H17	0.04	0.32	C17	0.01	-0.32	C17	-0.02	-0.38	H17	0.02	0.43
H18	0.03	0.15	H18	0.05	-0.40	H18	0.05	-0.15	C18	0.01	0.51
H19	0.03	-0.01	H19	0.03	0.06	H19	0.04	0.09	C19	0.02	0.30
H20	0.05	0.58	H20	0.02	0.21	H20	0.03	0.14	H20	0.00	0.01
H21	0.05	0.41	H21	0.04	0.12	H21	0.05	-0.19	H21	0.05	0.31
H22	0.04	0.07	H22	0.05	0.06	H22	0.05	-0.29	C22	-0.01	-1.47
			H23	0.06	-0.41	H23	0.06	-0.23	H23	0.00	-0.14
			H24	0.05	-0.19	H24	0.06	-0.08	H24	0.04	0.55
			H25	0.05	-0.03	C25	0.05	0.52	C25	0.00	-0.02
						H26	0.00	0.08	H26	0.04	0.40
						H27	0.05	0.00	H27	0.02	0.11
						H28	0.03	0.02	H28	0.04	0.16
									H29	0.04	0.46
									H30	0.01	0.19
									H31	0.04	0.27

The site that might be available for nucleophilic attack is the one with a larger f_k^- value. On the other hand, the site that might be available for electrophilic attack is the one with a larger f_k^+ value. The results reported in Table 9 show that for nucleophilic attack, the highest f_k^- values of all inhibitors OXA1 to OXA4 are as expected for all the H atoms. Additionally, the C10 atom shows a larger positive value of f_k^- in OXA1 and OXA4; this carbon is the site that joins the two rings together. In OXA2 and OXA3, the sites with the largest f_k^- values are C11 and C12, respectively. This indicates the tendency to donate electrons to unfilled d -orbitals of the Fe atoms on the metal surface, and the distribution of the HOMOs agrees with this result. In contrast, the highest f_k^+ values of the four studied inhibitors are the O2/7 and N8 atoms, indicating that these sites are available for electrophilic attack during the electron back-donation process from the filled d -orbitals of the Fe atoms. Additionally, the distribution of the LUMOs agrees with this result [48]. Furthermore, the sum of the Fukui functions of all atoms in a molecule is equal to one [60].

Additionally, for each atom in the investigated molecules, the local softness (σ_f), local electrophilicity (ω_f), and local dual descriptors (Δf_k , $\Delta\sigma_f$, and $\Delta\omega_f$) were also calculated. The graphical representations of the dual Fukui descriptor (Δf_k), dual local softness ($\Delta\sigma_f$), and multiphilic descriptor ($\Delta\omega_f$) for the four investigated inhibitors are represented in Figure 5.



(a)

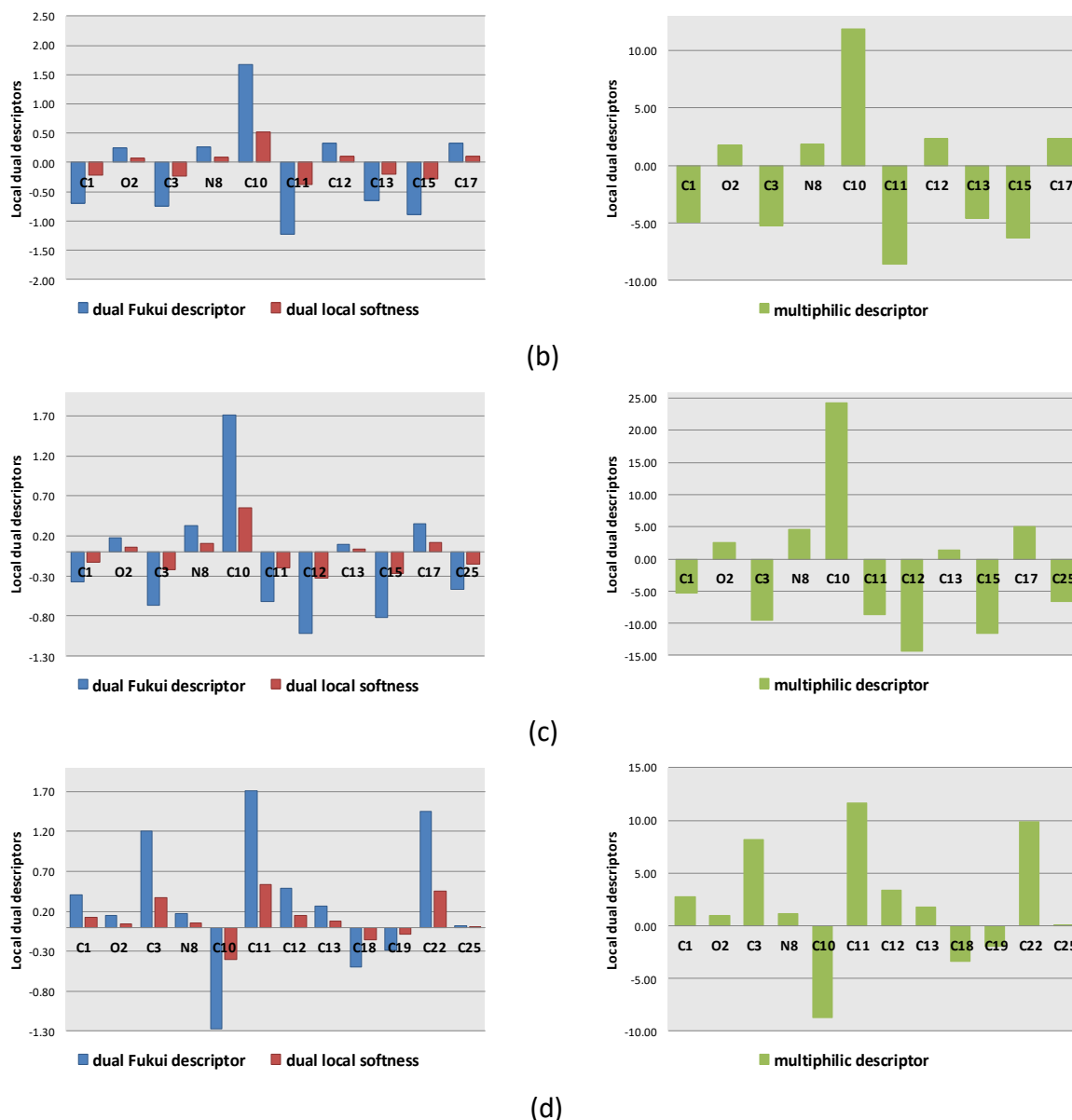


Figure 4. Graphical representation of the local dual descriptors, Δf_k , $\Delta\sigma_k$, and $\Delta\omega_k$, based on Fukui functions of the on C, N, and O atoms of the studied inhibitors: (a) OXA1, (b) OXA2, (c) OXA3, and (d) OXA4.

The local dual indices (Δf_k , $\Delta\sigma_f$, and $\Delta\omega_f$) indicate that the investigated inhibitors have several active sites. It is important to note that most sites of OXA2 and OXA3 show negative values for the three descriptors; some literature agrees with this finding. The negative values of the Fukui functions were attributed to the short interatomic distances encountered by atoms in a molecule [60, 61]. On the other hand, most sites in the OXA1 and OXA4 inhibitors show positive values for these descriptors (see Figure 5). Therefore, the latter two inhibitors have additional reactive sites for both nucleophilic and electrophilic attack compared to the aforementioned two inhibitors. Additionally, it can be proposed that the binding between the surface of the Fe and OXA1 and OXA4 is stronger than that in the case of OXA2 and OXA3. Finally, the abovementioned local descriptors reveal that the theoretical order for the

variation of inhibition efficiencies of the investigative inhibitors agrees to some extent with the available experimental data [48].

4. CONCLUSION

The corrosion inhibition efficiency of some synthesized oxazolidine-based compounds has been tested for API 5L X60 steel in 1 M HCl solutions at room temperature. The synthetic compounds are excellent inhibitors for steel corrosion and can provide an inhibition efficiency of up to 80 % in the acid solution. They adsorb on the steel surface to reduce charge capacitance and charge transfer at the interface, thus lowering the rate of the anodic and cathodic half-reactions at the steel-acid solution interface. Attachment of a cyclooctyl substituent to the oxazolidine parent structure provided the highest inhibition efficiency, while the lowest efficiency was provided by the cyclohexyl substituent. The oxazolidine-based compounds are concluded to be mixed-type inhibitors. In the complementary DFT calculations, the global and local reactivity descriptors were calculated for the four studied inhibitors to gain insight into some structural and electronic properties that are correlated with the inhibition efficiency of these molecules in the gas phase and aqueous solutions. Fukui functions show that the oxygen, nitrogen (in all inhibitors), C10 (in OXA1 and OXA4), and C11 (in OXA2 and OXA3) atoms will probably be the main adsorption sites. For the investigated inhibitors, most of their global molecular reactivity was not correlated very well with the experimental inhibition efficiencies because they were based solely on their HOMO and LUMO energies; thus, it is necessary for these oxazolidine derivatives to take into account another extra condition/s to define their inhibition ability, such as atomic charges and local descriptors.

ACKNOWLEDGMENTS

This work was supported by the Deanship of Scientific Research (DSR), King Abdulaziz University, Jeddah, under grant No. (D-128-130-1440). The authors, therefore, gratefully acknowledge the DSR for technical and financial support. Additionally, Nuha Wazzan acknowledges King Abdulaziz University's High-Performance Computing Centre (Aziz Supercomputer) (<http://hpc.kau.edu.sa>) for supporting the computational work described in this paper.

References

1. I.B. Obot, I.B. Onyeachu and A.M. Kumar, *Carbohydrate Polymers*, 178 (2017) 200.
2. A. Dutta, S.K. Saha, U. Adhikari, P. Banerjee and D. Sukul, *Corrosion Science*, 123 (2017) 256.
3. I.B. Obot, S. Kaya, C. Kaya and B. Tüzün, *Physica E: Low-dimensional Systems and Nanostructures*, 80 (2016) 82.
4. J. Haque, V. Srivastava, C. Verma and M.A. Quraishi, *Journal of Molecular Liquids*, 225 (2017) 848.
5. M.A. Chidiebere, L. Nnanna, C.B. Adindu, K. Oguzie, O. Beluonwu, O. Benedict and E.E. Oguzie, *International Letters of Chemistry, Physics and Astronomy*, 69 (2016) 74.
6. M.A. Chidiebere, C.E. Ogukwe, K.L. Oguzie, C.N. Eneh and E.E. Oguzie, *Industrial & Engineering Chemistry Research*, 51 (2012) 668.

7. N.K. Gupta, C. Verma, M.A. Quraishi and A.K. Mukherjee, *Journal of Molecular Liquids*, 215 (2016) 47.
8. I.B.O. M. Hadj Meliani, A. Sorrou, M. A. Benghalia, C. Fares, A. Khadraoui, and M.D. Z. Azari, 2017, 6 (2017).
9. D.I. Njoku, Y. Li, H. Lgaz and E.E. Oguzie, *Journal of Molecular Liquids*, 249 (2018) 371.
10. C.B. Adindu, M.A. Chidiebere, F.C. Ibe, C.E. Ogukwe and E.E. Oguzie, *International Letters of Chemistry, Physics and Astronomy*, 73 (2017) 9.
11. E.B. Ituen, O. Akaranta and S.A. Umoren, *Journal of Molecular Liquids*, 246 (2017) 112.
12. I.B. Obot and A. Madhankumar, *Materials Chemistry and Physics*, 177 (2016) 266.
13. S.A. Haladu, S.A. Umoren, S.A. Ali and M.M. Solomon, *International Journal of Electrochemical Science*, 12 (2017) 9061.
14. A. Singh, E.E. Ebenso and M.A. Quraishi, *International Journal of Electrochemical Science*, 7 (2012) 4766.
15. I.B. Obot, N.O. Obi-Egbedi and S.A. Umoren, *Corrosion Science*, 51 (2009) 1868.
16. M. Abdallah, *Corrosion Science*, 46 (2004) 1981.
17. M.S. Al-Otaibi, A.M. Al-Mayouf, M. Khan, A.A. Mousa, S.A. Al-Mazroa and H.Z. Alkathlan, *Arabian Journal of Chemistry*, 7 (2014) 340.
18. S.A. Umoren, O. Ogbobe, I.O. Igwe and E.E. Ebenso, *Corrosion Science*, 50 (2008) 1998.
19. C. Verma, L.O. Olanakanmi, E.E. Ebenso and M.A. Quraishi, *Journal of Molecular Liquids*, 251 (2018) 100.
20. M.L. Cohen, *Nature*, 406 (2000) 762.
21. D.K. Hutchinson, *Current Topics in Medicinal Chemistry*, 3 (2003) 1021.
22. Neha Pandit, Rajeev K. Singla and B. Shrivastava, *International Journal of Medicinal Chemistry*, 2012 (2012).
23. Y.W. Chin, A.A. Salim, B.N. Su, Q. Mi, H.B. Chai, S. Riswan, L.B. Kardono, A. Ruskandi, N.R. Farnsworth, S.M. Swanson and A.D. Kinghorn, *Journal of Natural Products*, 71 (2008) 390.
24. W.L. Wang, T.J. Zhu, H.W. Tao, Z.Y. Lu, Y.C. Fang, Q.Q. Gu and W.M. Zhu, *Chem Biodivers*, 4 (2007) 2913.
25. J. Obniska and K. Kamiński, *Acta poloniae pharmaceutica*, 63 (2006) 101.
26. K. Kamiński, J. Obniska and M. Dybała, *European Journal of Medicinal Chemistry*, 43 (2008) 53.
27. G. Bahrenberg, R. Frank, B. Henkel, R. Jostock, M. Reich, H. Schick and F. Theil, Substituted spiro compounds and their use for producing pain-relief drugs, in: I. Pat (Ed.), 2006.
28. J. Obniska, K. Kaminski and E. Tatarczynska, *Pharmacol Rep*, 58 (2006) 207.
29. M.S. Chande, R.S. Verma, P.A. Barve, R.R. Khanwelkar, R.B. Vaidya and K.B. Ajaikumar, *European Journal of Medical Chemistry*, 40 (2005) 1143.
30. M.T. Alhaffar, S.A. Umoren, I.B. Obot and S.A. Ali, *RSC Advances*, 8 (2018) 1764.
31. H. Faidallah, A.A. Saqer, K.A. Alamry, K. Khan, M.A.M. Zayed and S. Khan, Design, synthesis and biological evaluation of some novel hexahydroquinoline-3-carbonitriles as anticancer and antimicrobial agents, 2014.
32. N. Wazzan, I.B. Obot and H. Faidallah, *Journal of Adhesion Science and Technology*, 32 (2018) 2569.
33. S.A. Umoren, I.B. Obot, A. Madhankumar and Z.M. Gasem, *Carbohydrate Polymers*, 124 (2015) 280.
34. I.B. Obot, I.B. Onyeachu, N. Wazzan and A.H. Al-Amri, *Journal of Molecular Liquids*, 279 (2019) 190.
35. G.W.T. M. J. Frisch, H. B. Schlegel, G. E. Scuseria, M. A. Robb, J. R. Cheeseman, G. Scalmani, V. Barone, G. A. Petersson, H. Nakatsuji, X. Li, M. Caricato, A. Marenich, J. Bloino, B. G. Janesko, R. Gomperts, B. Mennucci, H. P. Hratchian, J. V. Ortiz, A. F. Izmaylov, J. L. Sonnenberg, D. Williams-Young, F. Ding, F. Lipparini, F. Egidi, J. Goings, B. Peng, A. Petrone, T. Henderson, D. Ranasinghe, V. G. Zakrzewski, J. Gao, N. Rega, G. Zheng, W. Liang, M. Hada, M. Ehara, K.

- Toyota, R. Fukuda, J. Hasegawa, M. Ishida, T. Nakajima, Y. Honda, O. Kitao, H. Nakai, T. Vreven, K. Throssell, J. A. Montgomery, Jr., J. E. Peralta, F. Ogliaro, M. Bearpark, J. J. Heyd, E. Brothers, K. N. Kudin, V. N. Staroverov, T. Keith, R. Kobayashi, J. Normand, K. Raghavachari, A. Rendell, J. C. Burant, S. S. Iyengar, J. Tomasi, M. Cossi, J. M. Millam, M. Klene, C. Adamo, R. Cammi, J. W. Ochterski, R. L. Martin, K. Morokuma, O. Farkas, J. B. Foresman, and D. J. Fox, Gaussian 09, Gaussian, Inc., Wallingford CT, 2016.
36. A.D. Becke, *Physical Review A*, 38 (1988) 3098.
 37. C. Lee, W. Yang and R.G. Parr, *Physical Review B*, 37 (1988) 785.
 38. V. Barone and M. Cossi, *The Journal of Physical Chemistry A*, 102 (1998) 1995.
 39. C. Maurizio, R. Nadia, S. Giovanni and B. Vincenzo, *Journal of Computational Chemistry*, 24 (2003) 669.
 40. L. Guo, C. Qi, X. Zheng, R. Zhang, X. Shen and S. Kaya, *RSC Advances*, 7 (2017) 29042.
 41. R.T. Loto, C.A. Loto, O. Joseph and G. Olanrewaju, *Results in Physics*, 6 (2016) 305.
 42. R.D. Bach, *Journal of the American Chemical Society*, 131 (2009) 5233.
 43. Y.G. Skrypnik, T.F. Doroshenko and S.Y. Skrypnik, *Materials Science*, 31 (1996) 324.
 44. E.E. Oguzie, Y. Li and F.H. Wang, *Journal of Colloid and Interface Science*, 310 (2007) 90.
 45. S.A. Umoren, M.M. Solomon, U.M. Eduok, I.B. Obot and A.U. Israel, *Journal of Environmental Chemical Engineering*, 2 (2014) 1048.
 46. C. Chu-nan, *Corrosion Science*, 22 (1982) 205.
 47. M. Stern and A.L. Geary, *Journal of the Electrochemical Society*, 104 (1957) 56.
 48. L. Guo, Z.S. Safi, S. Kaya, W. Shi, B. Tüzün, N. Altunay and C. Kaya, *Frontiers in Chemistry*, 6 (2018).
 49. N.A. Wazzan, *Journal of Industrial and Engineering Chemistry*, 26 (2015) 291.
 50. N.A. Wazzan, I.B. Obot and S. Kaya, *Journal of Molecular Liquids*, 221 (2016) 579.
 51. Roqaya H Albrakaty, Nuha A Wazzan and I. Obot, *International Journal of Electrochemical Science*, 13 (2018) 3535.
 52. N. Kovačević, I. Milošev and A. Kokalj, *Corrosion Science*, 98 (2015) 457.
 53. N.A. Wazzan, *Journal of Industrial and Engineering Chemistry*, 26 (2015) 291.
 54. N. Kovačević and A. Kokalj, *Corrosion Science*, 53 (2011) 909.
 55. F. Kayadibi, S.G. Sagdinc and Y.S. Kara, *Protection of Metals and Physical Chemistry of Surfaces*, 51 (2015) 143.
 56. B. Gómez, N.V. Likhanova, M.A. Domínguez-Aguilar, R. Martínez-Palou, A. Vela and J.L. Gázquez, *The Journal of Physical Chemistry B*, 110 (2006) 8928.
 57. M.A. Bedair, *Journal of Molecular Liquids*, 219 (2016) 128.
 58. R.T. Sanderson, *Journal of the American Chemical Society*, 105 (1983) 2259.
 59. N. Khalil, *Electrochimica Acta*, 48 (2003) 2635.
 60. L. Senthilkumar and P. Kollandaivel, *Molecular Physics*, 103 (2005) 547.
 61. P. Bultinck, R. Carbó-Dorca and W. Langenaeker, *The Journal of Chemical Physics*, 118 (2003) 4349.